Microfluid Nanofluid (2011) 10:1119–1125
DOI 10.1007/s10404-010-0740-y

ORIGINAL PAPER

An integrated silicon sensor with microfluidic chip for monitoring potassium and pH

Sanjiv Sharma · Anna Radomska-Botelho Moniz · Iasonas Triantis · Kostis Michelakis · Jakub Trzebinski · Alireza Azarbadegan · Benjamin Field · Chris Toumazou · Ian Eames · Anthony Cass

Received: 17 June 2010 / Accepted: 4 November 2010 / Published online: 1 December 2010
© Springer-Verlag 2010

Abstract We present ion-sensitive field effect transistor-based sensors, integrated with a microfluidic chip, for monitoring pH and potassium cations. The sensor is strategically located at the base of a well so that the response time of the device depends both on the mean flow through the device and the diffusion coefficient of the analyte being monitored. This would enable monitoring of ions in the presence of larger molecules. The dependence of the device response time on diffusive transport of analytes was examined through a numerical study of the flow field and the passive diffusion of a chemical species. The predicted device response time was compared with the experimental measurements and reasonable agreement found. The general dependence of device response time on geometry, flow rate, and analyte diffusion coefficient was derived. These devices can be used with biological fluids where monitoring of pH and cations provide vital information about the well-being of patients.

S. Sharma (✉) · A. R.-B. Moniz · I. Triantis · K. Michelakis · J. Trzebinski · C. Toumazou · A. Cass
Institute of Biomedical Engineering, Imperial College London, South Kensington Campus, Exhibition Road, London SW7 2AZ, UK
e-mail: s.sharma@imperial.ac.uk

B. Field
Department of Investigative Medicine, Imperial College London, Hammersmith Campus, Du Cane Road, London W12 0NN, UK

J. Trzebinski
Brunel Institute for Bioengineering, Brunel University, Uxbridge, West London UB8 3PH, UK

A. Azarbadegan · I. Eames
Mechanical Engineering Department, University College London, Torrington Place, London WC1E 7JE, UK

Keywords Microfluidic · ISFET · ChemFET · Computational fluid dynamics

1 Introduction

Since their introduction in 1970 by Bergveld (1972) as sensors for measuring ion concentration around nerve tissues (Bergveld 2003), ion-sensitive field effect transistors (ISFET) today are used in wide range of sensing applications in the fields of clinical medicine, biotechnology, and the environment (Schning 2002). Their attractive features, such as small size, fast response time, low cost, and multiple integration of various kinds of biologically active materials (e.g., enzymes, antibodies, DNA, and cells), make them well suited for Micro Total Analytical Systems (μTAS) or Lab-on-Chip devices (Reyes et al. 2002; Auroux et al. 2002). Integrating field effect devices with microfluidic platform allow manipulation of low volume samples and the realisation of high-performance detection systems with reduced size. Together they offer cheap and portable devices for real-time monitoring that could be used for various biomedical and point of care diagnostic applications.

The first attempt towards integrating microfluidics and field effect transistors was reported in 1999, referred to as flowFETs. These devices were used as controlling and switching elements in microfluidic networks (Schasfoort et al. 1999). Sharma et al. (2006) have reported silicon on insulator-based microfluidic device with monolithically integrated FETs for microTAS applications. An extended gate field effect transistor (EGFET)-based biosensor integrated with a silicon microfluidic channel for the electronic detection of streptavidin–biotin protein complexes has been reported by Kim et al. In this instance, gold was used

as the extended gate coated with self-assembled monolayers of thiols, on to which the biotin avidin complex was immobilized (Kim et al. 2006).

Truman et al. (2006) reported the use of silicon-based ISFETs for monitoring transport and chemical properties of liquids in microfluidic systems. Reliable, time-resolved ion, and molecular transport sensing in chemoreceptive neurons in microfluidic channels using transistors has been demonstrated by Jacquot et al. (2007). Tetraphenylborate derivatives have been used to modify ISFETs on polymeric microfluidic devices for sensing cationic surfactants in dental rinses (Masadome et al. 2006). In another instance, a microfluidic chip was used for cell culture and a large transistor-based sensor array chip for direct extracellular imaging (Milgrew et al. 2005). Literature survey does not reveal any solid state sensors integrated microfluidic device that could be used for simultaneous determination of cations.

In this study, the authors report on a novel design for a microfluidic device integrated with ISFET sensor. The novel aspect of the device design is that the device response time is sensitive to the diffusivity of the analyte species, thereby enabling it to exploit differences in diffusion coefficient between large and small molecules. This is achieved by locating the sensor at the base of a well which is placed below a hexagonal fluid chamber—the combination of these two aspects means that the flow above the sensor is sufficiently slow and hence the response time is largely controlled by diffusion. The authors present simulation studies of the fluid flowing through the channel, governed by the diffusion of the cations to the sensor surface, and look at the sensor response. The results from a detailed numerical study were compared with experiments involving different solutions (pH and potassium cations) at different concentrations and interpreted using a mathematical model. The results are then put into a general context in the conclusion.

2 Experimental and theoretical methodology

2.1 Fabrication

The ISFETs were obtained commercially from Sentron Europe. The devices are encapsulated, thereby exposing only the sensitive area of the ISFET, as seen in Fig. 1 (inset).

The multilayered microfluidic platform comprises a polydimethylsiloxane (PDMS) microfluidic chip, planar electrodes, and the sensing layer (Fig. 1). The PDMS chip was fabricated using a standard moulding technique as described earlier (Hofmann 2005) (Duffy et al. 1998). Sylguard 184 monomer and the curing agent (ratio 10:1)

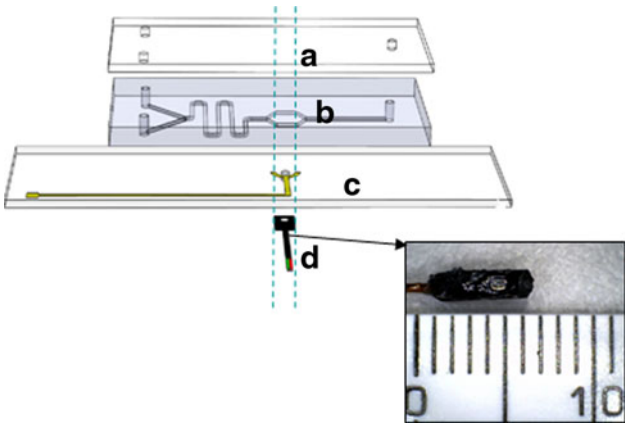

Fig. 1 Exploded view of the microfluidic. The device comprises **a** a glass cover plate for tubings, **b** a PDMS microchip, **c** a planar electrode with Au/Ti electrode on a glass slide with 1-mm hole for access to sensitive area of the ISFET, and **d** an ISFET sensor. The separation between the *vertical lines* in the inset is 1 mm. The *inset* shows an encapsulated ISFET and the geometry used in the computational study. As can be seen, the *black* encapsulation layer insulates the ISFET only exposing the sensitive gate surface

were poured into a photo-lithographically pre-fabricated SU-8 mould and left to cure overnight. The PDMS was the cut and peeled off the mould. This chip has two inlets with meanders leading to hexagonal chamber and finally terminates with an outlet. The microchannels are 1.0-mm wide and 1.0-mm deep.

The gold planar reference electrode on glass used for pH sensing was fabricated by standard photolithography and liftoff. AZ5214 photoresist was spun on a glass slide. Using a mask aligner and a photo mask, the areas where the gold electrodes are desired, were exposed and developed. The slide was then placed in an evaporator and 10 nm of Titanium and 40 nm of gold were deposited. The photoresist was stripped-off using acetone leaving the desired planar patterned gold electrode on the glass slide. For potassium sensing, the silver planar electrodes were fabricated in the same manner as described before with silver evaporated and later modified using $FeCl_3$ to obtain Ag/AgCl reference electrode.

The ISFET readout circuit used for these experiments was based on the circuit described by Bergveld (1972). The top amplifier, connected as a buffer, makes sure that the ISFET drain current and drain source voltage were fixed at 100 μA and 500 mV, respectively. In this so-called drain follower configuration, with the remote gate voltage grounded (reference electrode to ground), the voltage across the resistor R is equal to the source drain voltage V_{DS}. Since the current source is fixed and the V_{DS} was constant, the current sink determines the drain current and the source voltage can be sensed and fed to the output through the bottom amplifier. Thus, the source voltage is used to trace the gate potential variations due to the ionic concentration changes.

K^+ChemFETs were obtained by solvent casting of a conventional plasticized carboxylated polyvinyl chloride membrane (PVC-COOH) (66% w/w), containing valinomycin (1% w/w) and plasticiser (33% w/w) on the ISFET sensing membrane, after appropriately adapting existing protocol (Chudy et al. 2001).

The glass and PDMS layers were aligned and bonded together after their exposure to oxygen plasma for 1 min at a pressure of 0.8 mBar using an oxygen plasma instrument (Diener Technologies). The encapsulated ISFET and K^+ChemFET were attached to the microfluidic system using Araldite instant clear epoxy adhesive. These K^+ChemFETs were found to be stable for 1 week and could be stripped off the microfluidic platform using a surgical blade and replaced by new ones.

2.2 Numerical simulation of fluid flow and ion diffusion

The purpose of the computational study was to examine the influence of flow rate and ion diffusivity on the response of the device to changes in ion concentration.

These transport process were analysed using a commercially available software package (ANSYS CFX 5.0). The flow was assumed to be incompressible, isothermal and to consist of water at 25°C whose properties are (dynamic viscosity 8.9×10^{-4} kg/ms and density 997 kg/m^3). The transport of ions (H^+ and K^+) was modelled based on the realistic assumption that they were passive (and did not affect the fluid properties), whose evolution could be described by a linear advection diffusion equation with a diffusivity which is independent of the ion concentration. These assumptions are realistic for this problem. The characteristic Reynolds number of the flow $Re = Q/hw$ was low ($\sim$1–10) so that the flow is steady and symmetric about a mid vertical plane. To reduce computation burden, reflectional symmetry was employed and after discretising the domain gave a mixed grid with 223756 elements. The diffusive transport process was analysed by initialising the whole concentration field with $\hat{C} = 1$ and placing an inlet condition of $\hat{C} = 0$. The sweeping of material from the well provided a clear indication of how the flow rate and diffusivity affected changes in concentration at the base of the well ($\hat{C}_S$). The flow in the computational model was defined in terms of an inlet (top-hat) flow field normal to the inlet plane and a zero gauge pressure on the outlet plane.

2.3 Device operation

A schematic of the integrated device is shown in Fig. 1. The platform consists of a top glass cover plate that allows interfacing with a peristaltic/syringe pumps via tubings. Below the glass cover plate is the PDMS microfluidic chip. The central hexagonal part of the microfluidic chip (of width $w_H = 5$ mm) provides the necessary chamber volume and sits above the planar reference electrode and the active gate area of the ISFET. The solution in the microfluidic chip comes in contact with the sensitive area of the ISFET through the 1-mm hole drilled on the glass slide.

2.4 Measurements

The functioning of the chemical sensor was demonstrated by testing the H^+ ion detection properties. Potential hydrogen (pH) measurements were studied using three standard buffer solutions (pH 4.0, 7.0, and 10.0). All the measurements were performed at a constant temperature (20°C) in a beaker, against both Au, and Ag/AgCl reference electrodes.

The K^+ChemFETs were obtained by modifying ISFETs as described before. These K^+ChemFETs were used for titrations with solutions in the range of 10^{-4} to 10^{-1} M. Titrations were done in pure DI water and PBS saline solutions. All potentials were measured against an Ag/AgCl reference electrode. The K^+ChemFET s was operated at constant drain current, $I_{DS} = 100$ μA and constant drain-source voltage, $V_{DS} = 500$ mV.

The ISFET-based microfluidic device was connected to a syringe pump. Different pH solutions were pumped through the device at flow rates of $Q = 100$, 250, and 500 μl/min. Devices with K^+ChemFET were connected to syringe pumps and KCl salt solutions pumped in the device in the range of 1 μM–1 M potassium concentration at flow rates of 100, 125, and 250 μl/min. A National Instruments data acquisition module was used with LabView program to collect data at 100 Hz. The measured time-series enabled the response time of the device t_D corresponding to the time its takes for the voltage (or pH) to reach 90% of its final value. This time is proportional to the (e^{-1}) response time of the normalised concentration ($\hat{C}_S$), where $t_D \sim 4t_R$.

3 Results and discussion

The main objective of this study is to demonstrate functional integration of encapsulated ISFET-based sensors with microfluidic platforms. In the process, the authors have introduced a device design comprising a sensor that is located orthogonal to the microchannel. The fluid flows perpendicular to the sensor and the cation diffuse through a 1-mm diameter, 1-mm deep cylindrical well.

3.1 Solid state sensors integrated to microfluidic chip

The potentiometric response of the microfluidic device with ISFET sensor for flow rates of 100, 250, and 500 μl/min for the three pH solutions is depicted in Fig. 2. The sensitivity values measured are 49.67, 48.83, and 34.72 mV/pH unit, respectively. The microfluidic device with ISFET sensor shows a good response for different pH solutions at flow rates of 100 and 250 μl/min. Higher flow rates affect the sensor performance as evident from the response time data for 500 μl/min. This could be attributed to a diffusion limiting step because of a shorter residence time of the fluid in the chamber.

The K^+ChemFET sensor showed a good potentiometric response to manual as well as syringe-based injections of various potassium concentrations varying from 10^{-2} to 10^{-6} M. Above a KCl concentration of 10^{-2} M, the device is weakly dependent on concentration because at higher concentrations the sensor surface gets saturated with potassium ions making detection difficult.

The characteristic response time of the device for different flow rates was estimated from the response curves by examining the time taken for the measured potentiometric response to reach a steady value following a change in species concentration. Figure 3 shows the variation of the response time with flow rate.

3.2 Simulation of fluid dynamics

Transient simulations were undertaken using the same geometry as the experiments and flow rates of $Q = 50$, 100, 250, and 500 μl/min for H^+ (or K^+). The ions were treated as passive material whose spreading is described by a linear advection–diffusion equation characterised by a constant diffusion coefficient. A concentration C_∞ of ions was injected into the device with had an initial concentration of C_0; the normalised concentration $\hat{C} = (C - C_0)/(C_\infty - C_0)$, which takes values between 0 and 1 was calculated as a function of time and position. The concentration field at the base of the sensor well, C_S, was calculated, and from this the pH $\mathrm{pH} = -\log_{10} C$.

Figure 4 shows a table of the concentration field $\hat{C}$ for H^+ in water for contrasting times and volume flow rates. The normalised concentration field at the midpoint of the base of the well $\hat{C}_S$ was calculated as a function of time and is taken as a proxy measure of the concentration at the sensor surface. Figure 5a illustrates the typical variation of $\hat{C}_S$ (for protons) with time for different flow rates, which confirmed the exponential decay in $\hat{C}_S$ with time. Lines of best fit, of the form $\hat{C}_S = \exp(-(t - t_0)/t_R)$, where t_0 is the time the normalised concentration starts to decay, were calculated for the period after which the concentration field

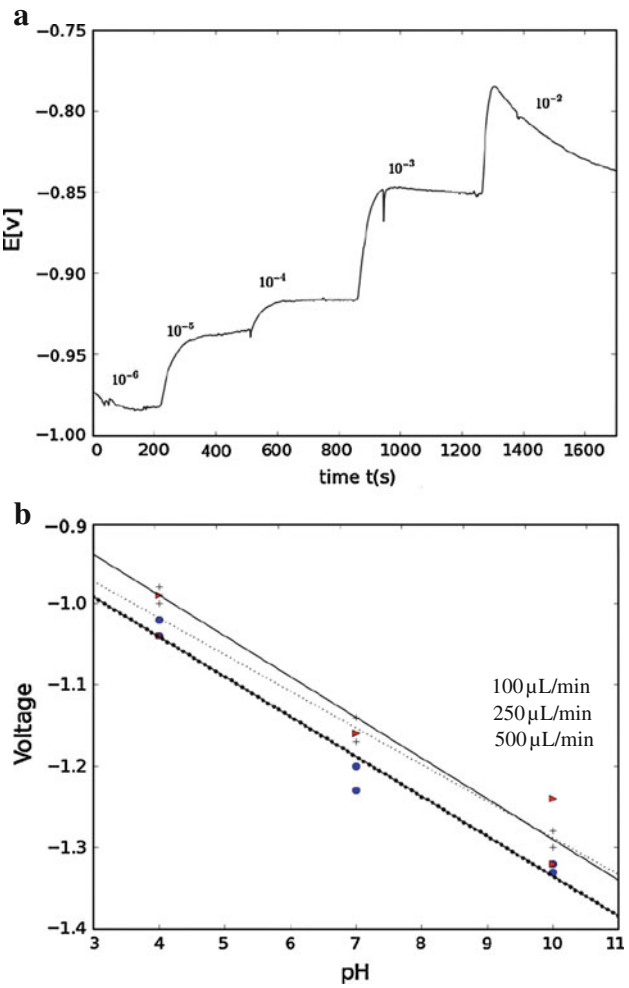

Fig. 2 **a** Potentiometric response of microfluidic devices for fixed flow rates $Q = 100$ μl/min, for K^+ChemFET. The concentration of KCl in M is given in the graph. **b** This shows the calculation curve for the pH sensor for different flow rates, the *red triangles* represent flow rate of 500 μl/min; the *blue circle* represents 250 μl/min; while the *crosses* represent flow rate of 100 μl/min. The trend lines for 100, 250, and 500 μl/min are shown by the *dotted*, *straight*, and *thick dotted lines*

began to decay. Figure 5bi and bii together shows the difference between how the ion concentration and pH approach saturated values, with the response time of the pH curve being approximately four times longer than the concentration curve. Figure 3 also shows the variation of the calculated response time t_R as function of flow rate and species type as predicted by numerical studies.

To understand the effect of diffusion on the transport from the top of the well to the sensor, the authors first consider diffusive transport described by $\partial\hat{C}/\partial t = D\partial^2\hat{C}/\partial y^2$, where y is in the vertical direction and D is the diffusion coefficient. For long time, the solution takes the form $\hat{C} \sim \exp(-t/t_R)f(y)$, where the slowest decaying solution has the form $1/t_R = (\pi/2)D/h_w^2$, where h_w is the

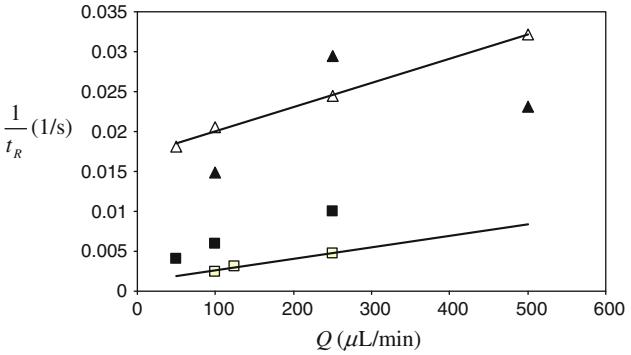

Fig. 3 A comparison between the difference response times in the ion concentration are plotted for the experiments and numerical calculations. The *fully shaded symbols* represent experimental measurements, while the *unshaded symbols* represent numerical simulations. *Triangles* represent potassium cation, while *squares* represent pH measurements

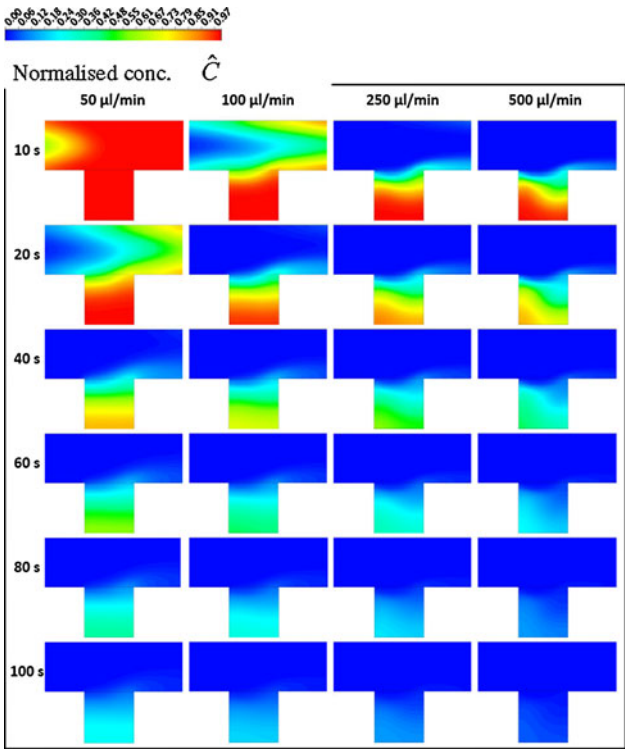

Fig. 4 Matrix of solutions showing the normalised concentration field ($\hat{C}$) in a midplane through the well at different times and flow rates

depth of the well. The effect of advection is to increase the rate of material being transported from the region above the well to the sensor head. The channel widening in the hexagonal chamber (from a channel width w to w_H, where $w_H/w = 5$) decreases the mean flow above the well head from $\bar{U} = Q/wh$ (where $h = 1$ mm is the channel depth) to $(w/w_H)\bar{U}$. The characteristic velocity within the well is a fraction of this, $\lambda(w/w_H)\bar{U} = \lambda Q/w_H h$. Since the flow in the well is driven by the shear stress at the top of the well where the flow adjusts from non-slip to slip, $\lambda \ll 1$, which gives a characteristic advective timescale, $h_W w_H h/\lambda Q$. A harmonic mean of the two characteristic timescales based on advection and diffusion provides an appropriate estimate of the response of the device to changes in the concentration. In total, this gives,

$$\frac{1}{t_R} = \frac{\pi D}{2h_W^2} + \frac{\lambda Q}{h_W w_H h}. \quad (1)$$

Equation 1 enables the responsiveness of the device to be expressed in terms of the geometry of the device, flow rate and diffusivity of the species. Figure 3b shows the variation of $1/t_R$ with Q and confirms, for the numerical calculations, the linear increase of increase response time with flow rate. The gradient of the linear fits for the pH and KCl simulations are the quite similar ($1.7 \times 10^6 Q$ (for pH) and $1.8 \times 10^6 Q$ (for KCl)). This suggests that $\lambda \sim 10^{-2}$. The intercept with the vertical axis provides an indication of pure diffusive transport. The authors estimated the values as $D = 1.5 \times 10^{-9}$ m^2/s (KCl) and $D = 10^{-8}$ m^2/s (pH), giving predicted intercepts (from 1) of 2.3×10^{-3} and 0.016, which compares well with the intercepts from the numerical results of 2.8×10^{-3} and 0.017, respectively. The discrepancy between experimental and numerical values appears to be greater for the protons. A plausible reason might be that protons diffuse by Grotthuss mechanism which might not be accurately reflected by the diffusion coefficient value used for the numerical studies.

4 Conclusions

We have developed a novel integrated microfluidic device which through its design is both sensitive and capable of discriminating between large and smaller ions with different diffusivities. The advection effect is substantially reduced as a consequence of both the divergent hexagonal section above the 1-mm diameter well head and the sensor located at the base of a well. Both of these design features ensure that the primary mode by which ions reach the sensors is dominated by diffusion. The novel feature is that recording a time series of the potentiometric response can enable suitably calibrated devices to discriminate between different species injected, mainly because the sensor response time is much faster than the ability of molecules to be introduced to the sensor surface.

The detailed computational study has shown that the ion concentration at the sensor surface has an exponential decay with a characteristic response time t_R whose dependence on device geometry was analysed and this is broadly confirmed by analysis of the potentiometric data.

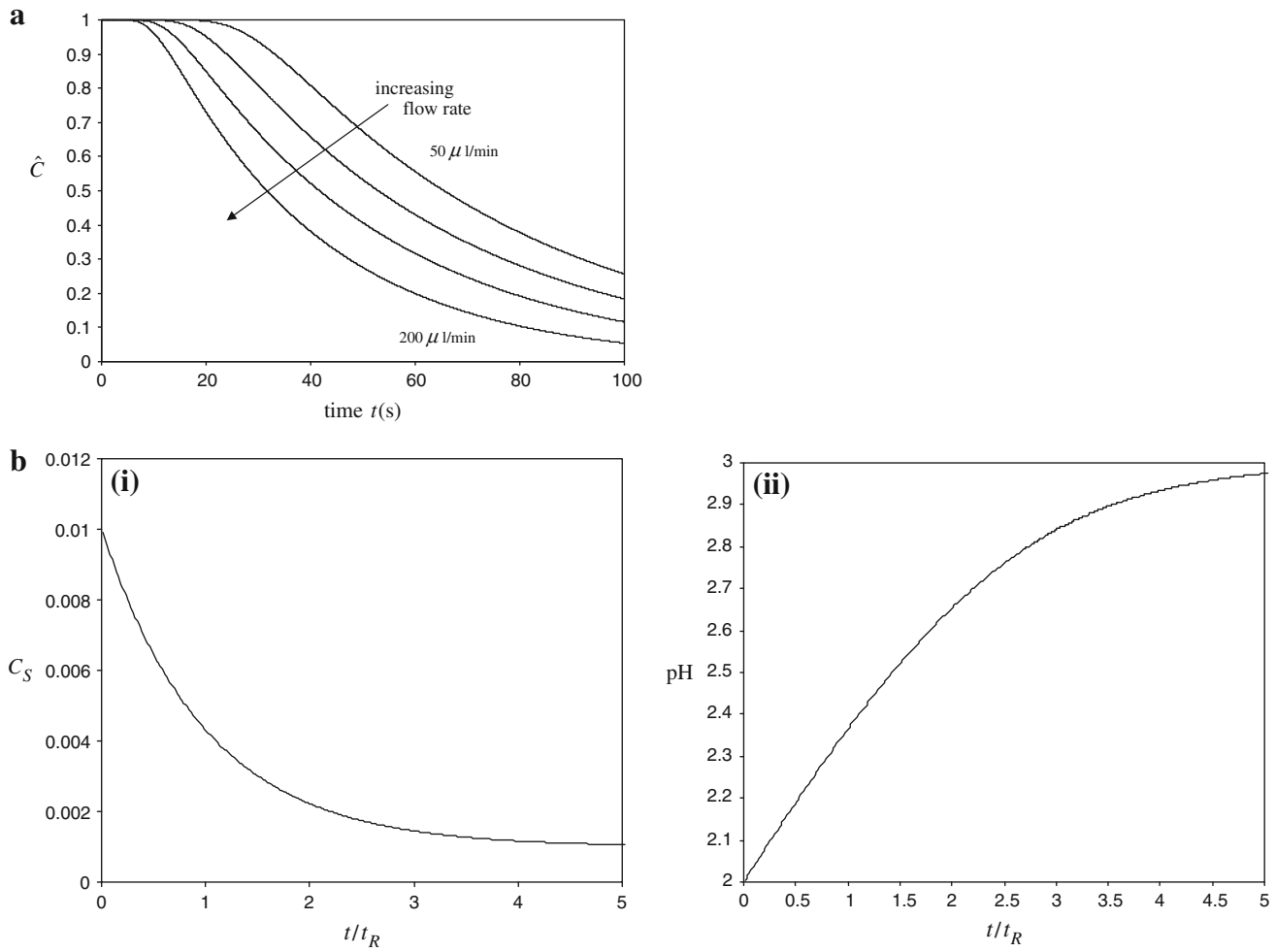

Fig. 5 **a** The variation of the normalised concentration $\hat{C}_S$ at the base of the well with time, for contrasting flow rates ($Q = 50$, 100, 250, and 500 μl/min). A log-linear plot confirms the exponential decay for large time, of the form $A\exp(-t/t_R)$ the ion concentration at the base of the well is plotted for dimensionless time in (**bi**) for the case when ions with concentration 10^{-2} are displaced by ions of concentration 10^{-3}. The corresponding change in pH is shown in (**bii**). In both the cases the flow rate is 100 μl/min

This supports the view that other physical processes might be important, such as density effects, which can be important over the long response times measured.

Although the response time of the silicon-based sensors increases when integrated to the microfluidic platform, this configuration possesses some major advantages. The ISFETs with Au reference electrode show an increased sensitivity (49.67 mV/pH unit) when integrated into a microfluidic platform compared to when used in bulk (33.27 mV/pH unit).This could be attributed to the efficient mass transport, in this case through the 1-mm diameter cavity between the microfluidic system and the sensor surface. With highly sensitive potentiostats capable of detecting 0.5 mV changes this would enable measurement of change in $\sim$0.01 unit of pH to be resolved. Moreover, this device enables the measurement of potassium cations in the range of 10^{-3} M to 10^{-6} M. The ability of the device to facilitate differential migration of analytes based on diffusion coefficients can allow measurement of cations in biological fluids without the need for major sample pre-treatments for larger molecules.

Acknowledgments The authors wish to acknowledge Vlady Bystrykivskyy for the designing of the device schematic and Suresh Vishwanathan Chettiar for help with clean-room fabrications. The authors acknowledge the use of the UCL *Legion* High Performance Computing Facility, and associated support services, in the completion of the computational aspect of this study.

References

Auroux PA, Iossifidis D, Reyes DR, Manz A (2002) Micro total analysis systems. 2. Analytical standard operations and applications. Anal Chem 74(12):2637–2652. doi:10.1021/Ac020239t

Bergveld P (1972) Development, operation, and application of the ion-sensitive field-effect transistor as a tool for electrophysiology. IEEE Trans Biomed Eng 19(5):342–351

Bergveld P (2003) Thirty years of isfetology—what happened in the past 30 years and what may happen in the next 30 years. Sens Actuator B 88(1):1–20

Chudy M, Wróblewski W, Dybko A, Brzózka Z (2001) Multi-ion analysis based on versatile sensor head. Sens Actuators B 78(1–3):320–325

Duffy DC, McDonald JC, Schueller OJA, Whitesides GM (1998) Rapid prototyping of microfluidic systems in poly(dimethylsiloxane). Anal Chem 70(23):4974–4984

Hofmann O (2005) Towards microalbuminuria determination on a disposable diagnostic microchip with integrated fluorescence detection based on thin-film organic light emitting diodes. Lab Chip 5(8):863–868

Jacquot BC, Lee C, Shen YN, Kan EC (2007) Time-resolved charge transport sensing by chemoreceptive neuron mos transistors (cvmos) with microfluidic channels. IEEE Sens J 7(9–10):1429–1434

Kim SM, Sommer GJ, Burns MA, Hasselbrink EF (2006) Low-power concentration and separation using temperature gradient focusing via joule heating. Anal Chem 78(23):8028–8035

Masadome T, Yada K, Wakida SI (2006) Microfluidic polymer chip integrated with an ISFET detector for cationic surfactant assay in dental rinses. Anal Sci 22(8):1065–1069

Milgrew MJ, Riehle MO, Cumming DRS (2005) A large transistor-based sensor array chip for direct extracellular imaging. Sens Actuator B 111:347–353

Reyes DR, Iossifidis D, Auroux PA, Manz A (2002) Micro total analysis systems. 1. Introduction, theory, and technology. Anal Chem 74(12):2623–2636. doi:10.1021/Ac0202435

Schasfoort RBM, Schlautmann S, Hendrikse L, van den Berg A (1999) Field-effect flow control for microfabricated fluidic networks. Science 286(5441):942–945

Schning M (2002) Recent advances in biologically sensitive field-effect transistors (biofets). Analyst 127(9):1137–1151

Sharma S, Buchholz K, Luber SM, Rant U, Tornow M, Abstreiter G (2006) Silicon-on-insulator microfluidic device with monolithic sensor integration for Mu-TAS applications. J Microelectromech Syst 15(2):308–313

Truman P, Uhlmann P, Stamm M (2006) Monitoring liquid transport and chemical composition in lab on a chip systems using ion sensitive FET devices. Lab Chip 6(9):1220–1228